CLINICAL RESEARCH
Heart failure/cardiomyopathy

Left ventricular dyssynchrony in patients with left bundle branch block and patients after myocardial infarction: integration of mechanics and viability by cardiac magnetic resonance

Andrea K. Rutz[1†], Robert Manka[1,2†], Sebastian Kozerke[1], Susanne Roas[3], Peter Boesiger[1], and Juerg Schwitter[3]*

[1]Institute for Biomedical Engineering, University and ETH Zurich, Zurich, Switzerland; [2]Department of Internal Medicine/Cardiology, German Heart Institute Berlin, Berlin, Germany; and [3]Clinic of Cardiology, University Hospital Zurich, Raemistrasse 100, CH-8091 Zurich, Switzerland

Aims	To quantify left ventricular (LV) dyssynchrony in patients with left bundle branch block (LBBB) and in patients after myocardial infarction (MI) applying an accelerated three-dimensional (3D) tagging cardiac magnetic resonance (CMR) technique, and to combine dyssynchrony information with viability data obtained by late gadolinium enhancement (LGE) CMR.
Methods and results	Thirty-two patients (59 ± 11 years) after first MI (Pats_{MI}), 10 patients (63 ± 10 years) with LBBB (ejection fraction $< 40\%$; $\text{Pats}_{\text{LBBB}<40}$), 13 patients ($63 \pm 11$) with LBBB (ejection fraction $\geq 40\%$; $\text{Pats}_{\text{LBBB}\geq40}$), and 15 healthy controls (53 ± 10 years) underwent 3D tagging CMR and LGE imaging at 1.5 T. As a measure of mechanical LV dyssynchrony, the standard deviation of T_{max} over the LV, the circumferential uniformity ratio estimate (CURE) index, and a segmental-based circumferential systolic dyssynchrony index (SDI) were calculated. All three parameters detected significantly increased circumferential dyssynchrony in patients compared with controls. The CURE and SDI showed a good correlation ($r = 0.93$, $P < 0.0001$) and detected most severe dyssynchrony in $\text{Pats}_{\text{LBBB}<40}$ ($P < 0.001$ vs. controls, $P < 0.005$ vs. Pats_{MI}). Systolic dyssynchrony index additionally allowed integration of localized viability information to yield $\text{SDI}_{\text{viable}}$ which was highest in $\text{Pats}_{\text{LBBB}<40}$.
Conclusion	Dyssynchrony patterns in the LV can be quantified globally and regionally by 3D tagging CMR. Combination of viability and dyssynchrony information allows for a comprehensive dyssynchrony quantification in patients with LBBB or post-MI. Future studies are required to test the value of the method to predict responsiveness to resynchronization.
Keywords	Magnetic resonance imaging • Tagging • Myocardial infarction • Left bundle branch block • Dyssynchrony • Cardiac resynchronization therapy

Introduction

Conduction disturbances as well as ischaemia or scar in the left ventricular (LV) myocardium have been shown in animals and humans to cause dyssynchrony and intraventricular unloading phenomena.[1–4] Congestive heart failure patients with features of dyssynchrony are therefore benefiting from cardiac resynchronization therapy (CRT). Cardiac resynchronization therapy has proved successful in large patient populations, but ~20–30% of patients do not appear to respond to CRT[5] applying current patient selection criteria which mainly consider symptoms, global LV ejection fraction (LVEF), and QRS duration.[6] In addition, more sophisticated approaches using echocardiography to quantify LV dyssynchrony yielded contradictive results.[7–9] Therefore, a better understanding of the mechanisms involved in the various forms of intraventricular dyssynchrony is needed.

†The first two authors contributed equally to the study.

* Corresponding author. University Hospital Lausanne – CHUV, Cardiology, Switzerland. Tel: +41 21 314 0015, Secretariat: +41 21 314 0010, Fax: +41 21 314 0013, Email: jurg.schwitter@chuv.ch

Cardiac magnetic resonance (CMR) offers the possibility to acquire motion-encoded data sets with high temporal resolution using sophisticated tagging techniques, which can differentiate local tissue deformation from bulk cardiac motion or tethering.[10–12] While conventional, two-dimensional techniques are limited in practical use by long scan times and slice registration problems, a novel method was recently introduced,[13] which allows measuring three-dimensional (3D), tagged volumes covering the entire LV in less than 2 min examination time. Novel post-processing algorithms such as harmonic phase (HARP) analysis[14] and its modifications[15] allow 3D strain maps to be analysed in very short times. And finally, CMR can provide accurate high-resolution viability information in the entire LV.[16,17]

A large variety of different mechanical[18,19] and temporal[3,11] CMR tagging parameters has been suggested to describe dyssynchrony and several parameters have been validated in animal models.[12] A most promising parameter, the circumferential uniformity ratio estimate (CURE)[12,18,20] (also called TUS: temporal uniformity of strain), readily predicted the responsiveness to CRT in dog experiments. However, this approach utilizing the CURE index is hampered by the fact that dyssynchrony is lumped into one value (1 = perfect synchrony; 0 = complete dyssynchrony), thus, the information of location of dyssynchrony in the LV is no longer available. Consequently, the presence of dyssynchrony cannot readily be linked to the presence and distribution patterns of scar in the LV, which has been shown to be crucial for the prediction of CRT success.[21]

Accordingly, the aims of this study were: (i) to transfer the tagging approach that was proved successful in canine experiments into humans with both preserved and reduced LV function and to further characterize the dyssynchrony patterns caused by either left bundle branch block (LBBB) or ischaemic heart disease with scarring; (ii) to improve the assessment of dyssynchrony allowing for the integration of viability information into the 3D data sets; and (iii) finally in order to be clinically applicable, to assess the inter-study, the inter-observer, and the intra-observer reproducibility of these measurements.

Methods

Study population

The study protocol was approved by the local Ethics Committee and all subjects gave written informed consent before study participation. Between October 2006 and January 2009, 35 patients with LBBB [without a history of coronary artery disease (CAD) and myocardial infarction (MI) or valve disease; Pats$_{LBBB}$] were screened for this study. Eight patients with atrial fibrillation or an implanted pacemaker were excluded. Four patients refused participation in the current study. In order to describe and quantify LV dyssynchrony in Pats$_{LBBB}$ with preserved and reduced LV function, the remaining 23 Pats$_{LBBB}$ were divided into a group with reduced LVEF (10 Pats$_{LBBB<40}$ with an ejection fraction < 40%) and preserved LVEF (13 Pats$_{LBBB\geq40}$ with an ejection fraction ≥ 40%). All patients with LBBB and reduced function (Pats$_{LBBB<40}$) had an invasive coronary angiography to exclude CAD (within 1 year of the CMR study) characterizing them as dilative cardiomyopathy patients. To study the dyssynchrony pattern in ischaemic heart disease, an additional 32 patients were examined between November 2006 and November 2008 by CMR 9.6 ± 8 days after their first MI (Pats$_{MI}$).

In LBBB, the lateral wall typically exhibits a delayed contraction, thereby causing a stretching of the septum in early diastole. A similar pattern of post-systolic stretching of the antero-septal wall is observed in patients after antero-septal MI.[2] Therefore, dyssynchrony patterns were specifically compared between LBBB and patients with antero-septal MI to study the effect of integration of viability information in the overall assessment and quantification of LV dyssynchrony. Finally, between April 2007 and February 2008, 15 age-matched healthy volunteers (without a history or symptoms of cardiovascular disease) were recruited from a general practitioner and served as the control group (Controls). Exclusion criteria for study participation were contra-indications to CMR (typically incompatible metallic implants, claustrophobia). Seventy-one subjects of this study cohort successfully completed the CMR scans and 70 were included in the final analysis (drop-out: one inadequate tagging analysis). More detailed demographic and cardiac characteristics of each study group are listed in *Table 1*.

Data acquisition

The complete imaging protocol is shown schematically in *Figure 1*. All measurements were performed on a 1.5 T MRI scanner (Achieva, Philips Healthcare, Best, The Netherlands). After acquiring survey images and calibration data, short-axis images covering the entire LV were acquired using a steady-state free precession (SSFP) sequence (cardiac phases = 20, temporal resolution = 45 ms, slice thickness = 8 mm, 13–16 contiguous slices during repetitive breath-holds) to assess global LV function. An additional SSFP measurement with higher temporal resolution (cardiac phases = 50, temporal resolution = 17.6 ms, slice thickness = 8 mm) was performed through the aortic valve to determine timing of aortic valve closure (AVC).

For 3D tagging data, a novel, accelerated acquisition scheme with Complementary spatial modulation of magnetization was applied[13] requiring three breath-holds of 18 RR intervals duration each to cover the entire LV. Complementary Spatial Modulation of Magnetization acquisition provides a longer tag persistence into diastole, increases signal-to-noise ratio, is available on most MR machine types and can be modified to the 3D approach with minor changes. For read-out, a modified hybrid multi-shot, segmented echo-planar sequence was employed (field-of-view = $108 \times 108 \times 108$ mm^3, voxel size per encoding direction = $3.9 \times 7.7 \times 7.7$ mm^3, echo time = 3.3 ms, tag distance = 7 mm). Depending on the heart rate, 19–25 time frames were recorded with a temporal resolution of 27–37 ms and a final flip angle of 18–25°. To allow for tagging data registration, acquisition of the second and third data set was only started, if the diaphragm position was within a pre-defined window of 15 mm of the first breath-hold as measured by a navigator echo.[22] Any difference within this 15 mm window was additionally corrected for.

Late gadolinium-enhanced short-axis images covering the entire LV were additionally acquired in all Pats$_{MI}$ 15 min after administration of a bolus of 0.25 mmol/kg body weight of Gadobutrolum (Gadovist, Bayer-Schering Pharma, Germany) using an inversion recovery segmented gradient echo sequence with inversion time set to null normal myocardium (field-of-view = 350×350 mm^2, pixel size = 1.5×1.5 mm^2, repetition time = 7.4 ms, echo time = 4.4 ms, slice thickness = 8 mm, no slice gap).

Data analysis

The 3D tagging data were post-processed with HARP[14,15] using an in-house software tool extended for the analysis of 3D tagging data.

Table 1 Demographics of study population

	Controls	Pats$_{LBBB\geq40\%}$	Pats$_{LBBB<40\%}$	Pats$_{MI}$	Overall P-value	P-value vs. Pats$_{LBBB<40}$	P-value vs. Pats$_{MI}$
n	15	13	10	32			
Male, n (%)	11 (73%)	6 (46%)	6 (60%)	27 (84%)	ns		
Age (years)	53 ± 10	63 ± 11	63 ± 10	59 ± 11	ns		
BMI (kg/m^2)	24.9 ± 2.3	27.7 ± 7.1	25.0 ± 3.3	26.9 ± 3.6	ns		
Heart rate (b.p.m.)	68 ± 12	65 ± 8	79 ± 17	73 ± 17	ns		
QRS width (ms)	—	143 ± 12*	149 ± 16$^{\parallel}$	92 ± 14	<0.0001		<0.0001*$^{,\parallel}$
CAD-IRA: LAD, n (%)	—	—	—	27 (84%)	—		
CAD-IRA: RCA/LCX, n (%)	—	—	—	5 (16%)	—		
LV-scar (% LV mass)	—	—	—	25.5 ± 10.1	—		
LV-EDV (mL)	136 ± 36	145 ± 48	177 ± 44	149 ± 50	ns		
LV-ESV (mL)	53 ± 13$^{\#}$	70 ± 30$^{\&}$	128 ± 41	96 ± 39	<0.0001	<0.001$^{\#,\&}$	<0.001$^{\#}$
LVEF (%)	60 ± 4°	53 ± 7$^{\&}$	28 ± 9^{+}	37 ± 10	<0.0001	<0.001$^{\circ,\&}$	<0.05$^{\circ,\&,+}$

CAD-IRA, infarct-related artery in coronary artery disease patients; LAD, left anterior descending coronary artery; RCA/LCX, right and/or left circumflex coronary artery; EDV, end-diastolic volume; ESV, end-systolic volume; LVEF, left ventricular ejection fraction. P-values for group-wise comparisons (equal to six possible comparisons) are Bonferroni corrected.
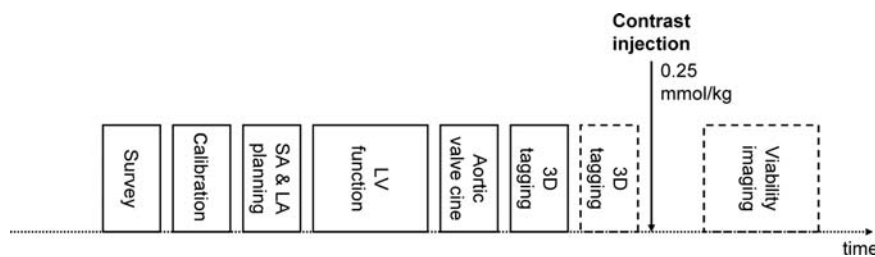

Figure 1 Imaging protocol. SA, short-axis cardiac views; LA, long-axis cardiac views. For inter-study reproducibility assessment, a second 3D tagging data set was acquired in five controls, five left bundle branch block patients, and five myocardial infarction patients. Viability imaging was only performed in MI patients (dashed boxes).

Eight to 11 short-axis mid-wall contours with a spacing of about 5° around the circumference were defined on slices covering the entire LV. The contours were subsequently HARP tracked[14,15] in 3D space through all time frames using peak combination.[15] The spatial resolution resulting from the 3D bandpass filtering in k-space was $9 \times 9 \times 9$ mm^3, characterizing the spatial blurring of the final displacement data. Mid-wall circumferential shortening (csh(t), in %) was defined as the length change of a contour at time t relative to the original length at end-diastole (first heart phase). For a detailed analysis of csh(t) in 48–66 segments of each LV, each mid-wall contour was divided into sectors of 60° starting at the anterior epicardial junction of the right and the left ventricles on the equatorial level and numbered consecutively from S1 to S6 in clockwise direction as viewed from the apex. For the segment-wise calculation of the shortening profiles, data were resampled at 10 cardiac levels in order to equalize the number of slices and thus the number of LV segments in all subjects. While the spatial resolution of the tagging approach results in a voxel size of ~0.27 g, the segment mass is ~2.0 g (average LV mass of 115 g divided by 60 segments).

The time to maximum csh, T_{max}, was automatically determined for each segment. To eliminate unreliable values of T_{max} due to akinesia or tracking artefacts, segments in which T_{max} was detected in the first three or in the last acquired time frame were inspected by an observer and corrected manually if necessary.[23] As a measure of mechanical LV dyssynchrony, the standard deviation (SD) of T_{max} over the LV was calculated[20] as well as the CURE index (details are given in Appendix and by Leclercq et al.[18]).

In order to obtain both, localized information about regional dyssynchronous motion and a global dyssynchrony estimate for the entire LV, a new parameter, the systolic dyssynchrony index (SDI), was calculated as described in Appendix. Since the SDI is sensitive for heterogeneous contractions towards the end of systole, high values will recognize late contracting segments, which would benefit from early pacing.

It was assumed that sectors with altered contraction and > 50% scar would not recover contraction even when perfectly synchronized. These sectors were therefore excluded from SDI calculation yielding a viability-corrected dyssynchrony parameter, i.e. SDI$_{viable}$.

Reproducibility

In order to assess inter- and intra-observer reproducibility, data analysis was performed in a blinded fashion 2 months after the original

analysis in randomly chosen patients (five Pats$_{MI}$ and five patients with LBBB) by the original observer (R.M.). An additional observer (A.K.R.) independently and blindly analysed the data using the same images in order to assess inter-observer reproducibility. Both readers had 4 years of experience with MR imaging methods.

For the assessment of inter-study reproducibility, the standard 3D tagging acquisition was performed twice in 15 randomly chosen subjects (five Controls, five Pats$_{MI}$, and five patients with LBBB). Reproducibility was calculated for CURE, SDI, and T_{max} SD.

Statistics

Statistical analysis was performed by using the SPSS software package release 15.0.1 (Chicago, IL, USA). Mean values $\pm$ SD were calculated for all groups. The paired Student's *t*-test or Wilcoxon test and independent samples *t*-test or Mann–Whitney test were used to test for differences within and between groups. All tests were two-tailed. The Kolmogorov–Smirnov test was used to test for normality. The results between the four study groups (*Tables 1 and 2*; *Figure 2*) were compared with an analysis of variance followed by Bonferroni *post hoc* testing considering six comparisons per parameter (InStat, 3.01, GraphPad Software Inc., San Diego, CA, USA). *P*-values less than 0.05 were considered statistically significant. Inter-study, inter-observer, and intra-observer reproducibility was evaluated by means of Bland–Altmann plots.[24] Linear regression analyses and partial correlation test by Pearson's method were done to assess relations.

The study was powered for the CURE index determined by 3D tagging CMR. We assumed from a previous study[20] a difference in CURE of 0.3 between controls and subjects with LBBB assessed by CMR. Considering a SD of 0.1, a sample size of $n = 3$ ($\alpha = 0.05$; power 90%) would be needed. Assuming a smaller difference in CURE of 0.2 with a SD of 0.1 between controls and patients after MI, a sample size of $n = 6$ ($\alpha = 0.05$; power 90%) would be needed. Larger patient groups were recruited to account for possible dropouts and a potentially higher variability of the SDI parameter, which was not known a priori. Owing to this lack of information, the sample size for the inter-study reproducibility assessment was arbitrarily set to 15 subjects. As this sample size is rather small, the 95% confidence intervals for the limits of agreement are also presented. For more robust calculations of sample sizes, e.g. for large clinical trials,

reproducibilities would probably need confirmation obtained with larger samples.

Results

Demographics

Demographics and cardiac characteristics of each study group are given in *Table 1*. The Pats$_{MI}$ group consisted of 32 patients, 18 (56%) of them with one-vessel disease, 9 (28%) with two-vessel disease, and 5 (16%) with three-vessel disease. The infarct-related artery was the left anterior descending coronary artery in 27 (84%) patients, the right coronary artery in three (9%) patients, and the left circumflex artery in two (7%) patients. Scar mass in the 32 patients was $25.5 \pm 10.1\%$ of the total LV mass.

Dyssynchrony in Controls, Pats$_{LBBB}$, and Pats$_{MI}$

Global LVEF was lowest in the Pats$_{LBBB<40}$ with $28 \pm 9\%$, i.e. in the patients with dilative cardiomyopathy ($P < 0.001$ vs. Controls), followed by the Pats$_{MI}$ with $37 \pm 10\%$ ($P < 0.05$ vs. Controls), while in Pats$_{LBBB\geq40}$ LVEF was only slightly reduced to $53 \pm 7\%$ (ns vs. Controls, *Table 1* and *Figure 2*). This pattern of reduced LV function is paralleled by the intraventricular circumferential dyssynchrony as assessed by the CURE index (lowest CURE values in Pats$_{LBBB<40}$) as shown in *Figure 2*. The proposed SDI shows a similar pattern with highest dyssynchrony in Pats$_{LBBB<40}$. The variance of T_{max} over all LV segments calculated by the SD was significantly greater in Pats$_{LBBB<40}$ and Pats$_{MI}$ ($P < 0.05$) compared with controls. In accordance with LVEF results, significantly reduced mean csh(AVC) over the entire LV could be detected in both Pats$_{LBBB<40}$ and Pats$_{MI}$ compared with Controls ($P < 0.05$; *Figure 2*). T_{max} mean (time to peak csh) was similar in Controls and Pats$_{MI}$, but was increased in the patients with LBBB ($P < 0.05$, *Figure 2*).

The correlation between the CURE and the SDI parameter was high ($r = -0.93$; $P < 0.0001$, *Figure 3*). The partial correlation coefficients were -0.69, -0.96, -0.95, and -0.87 for Controls, Pats$_{LBBB\geq40}$, Pats$_{LBBB<40}$, Pats$_{MI}$, respectively. The CURE–SDI

Table 2 Dyssynchrony and left ventricular function parameters

	Controls	Pats$_{LBBB\geq40\%}$	Pats$_{LBBB<40\%}$	Pats$_{MI}$
n	15	13	10	32
CURE	0.98 ± 0.01	0.92 ± 0.06	0.79 ± 0.15	0.90 ± 0.06
SDI	0.26 ± 0.07	0.55 ± 0.32	1.38 ± 1.30	0.70 ± 0.26
SDI$_{viable}$	0.26 ± 0.07	0.55 ± 0.32	1.38 ± 1.30	0.46 ± 0.18
T_{max} mean (ms)	336 ± 37	391 ± 30	406 ± 49	349 ± 34
T_{max} SD (ms)	47 ± 9	73 ± 17	102 ± 36	79 ± 11
LVEF (%)	60 ± 4	53 ± 7	28 ± 9	37 ± 10
csh(AVC) mean (%)	17.4 ± 2.2	15.5 ± 2.8	10.4 ± 3.8	11.1 ± 3.0
Tracking error (%)	5 ± 2	9 ± 4	8 ± 6	7 ± 3

For statistical comparisons, see *Figure 2*. In Pats$_{MI}$ the difference between SDI and SDI$_{viable}$ was significant (paired *t*-test, $P < 0.0001$). SDI$_{viable}$ in Pats$_{LBBB<40}$ was significantly higher than in Controls and Pats$_{MI}$ ($P < 0.0001$) and also higher than in Pats$_{LBBB\geq40}$ ($P < 0.01$, all *P*-values Bonferroni corrected for six comparisons). Tracking error of tagging data analysis, which indicates data quality, showed no significant differences between groups. One patient with LBBB was excluded from the analysis due to a tracking error in 26% of all tagging points.
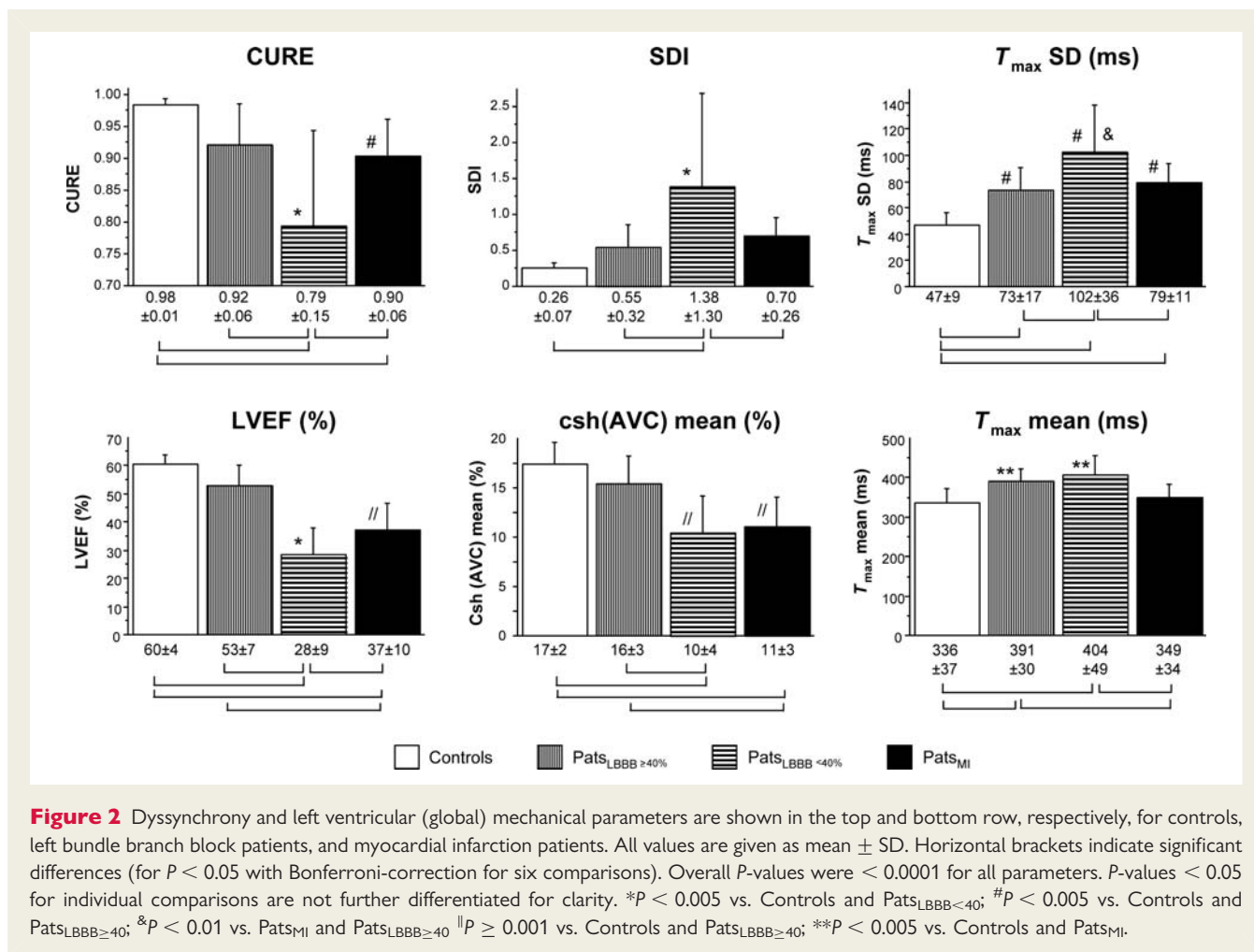
Figure 2 Dyssynchrony and left ventricular (global) mechanical parameters are shown in the top and bottom row, respectively, for controls, left bundle branch block patients, and myocardial infarction patients. All values are given as mean ± SD. Horizontal brackets indicate significant differences (for $P < 0.05$ with Bonferroni-correction for six comparisons). Overall P-values were < 0.0001 for all parameters. P-values < 0.05 for individual comparisons are not further differentiated for clarity. $^*P < 0.005$ vs. Controls and $Pats_{LBBB<40}$; $^{\#}P < 0.005$ vs. Controls and $Pats_{LBBB\geq40}$; $^{\&}P < 0.01$ vs. $Pats_{MI}$ and $Pats_{LBBB\geq40}$ $^{\|}P \geq 0.001$ vs. Controls and $Pats_{LBBB\geq40}$; $^{**}P < 0.005$ vs. Controls and $Pats_{MI}$.

relationship can also be described by the formula: $y = 11.6x^2 - 25.1x + 13.8$ (data not shown), which yields an r-value of -0.97 ($P < 0.0001$). Both formulas demonstrate an inverse relation between the two parameters; however, the number of data points (as shown in *Figure 3*) appears too small to definitely support a specific type of correlation. Moreover, LV scar mass and CURE correlated similarly as LV scar mass and SDI (*Figure 4*) in $Pats_{MI}$.

QRS duration showed a weak inverse correlation with LVEF in patients ($Pats_{LBBB}$ and $Pats_{MI}$) with reduced EF, i.e. below 40% ($r = 0.41$, $P < 0.03$, $n = 29$). In this population, QRS duration was positively correlated with SDI_{viable}, ($r = 0.59$, $P < 0.001$), but did not correlate with SDI ($P = 0.5$) or CURE ($P = 0.11$).

Results of one representative subject out of each study group (Controls, $Pats_{LBBB}$, and $Pats_{MI}$) are given in *Figure 5*. A patient after antero-septal infarction is shown to demonstrate the similarity with the LBBB dyssynchrony pattern. Both patients show increased SDI values (0.71 and 1.26, respectively) compared with the control (0.27). In the patient after MI, the infarcted segments show severely reduced (or absent) shortening during systole (*Figure 5G*). After AVC post-systolic shortening (equal to elastic recoil) of the infarcted segments begins immediately with relaxation of the non-infarcted (lateral) segments. The patient with LBBB shows a similar pattern with the septum (segment S6 in

Figure 5D) being even lengthened, i.e. stretched during late systole due to simultaneous contractions in the lateral wall. As in the MI patient, the septum of the LBBB patient begins to shorten in early diastole exactly at the time point when contraction in the lateral wall (segments S2−S4 in *Figure 5D*) terminates at AVC. Although in the MI patient this post-systolic shortening in the transmural scar region is reflecting an elastic recoil,[2] we may assume that this shortening in the septum of LBBB patients in early diastole is caused by an elastic recoil of viable myocardium.

In *Figure 6*, the Controls, the $Pats_{LBBB\geq40}$, and nine $Pats_{MI}$ with a medium-sized antero-septal infarction (scar mass 15−25% of LV mass) were averaged for the SDI parameter and are represented in the bull's eye plots. This figure shows a similar dyssynchrony pattern within the LV for $Pats_{LBBB}$ and $Pats_{MI}$ in agreement with the examples of *Figure 5*.

Incorporation of viability information into dyssynchrony assessment

While the dyssynchrony pattern for $Pats_{LBBB}$ and $Pats_{MI}$ with antero-septal MI was similar (example in *Figure 5* and averaged bull's eye plots in *Figure 6*), the expected maximum improvement in shortening with CRT in an individual segment would change, if
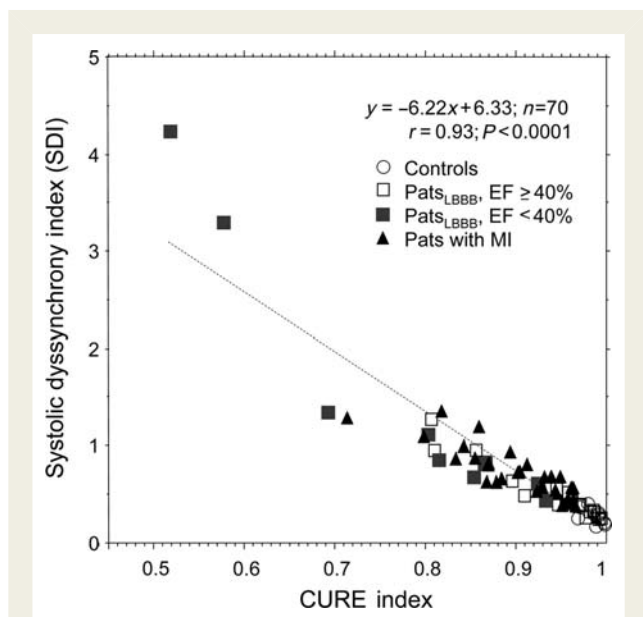
Figure 3 A high correlation was found between the circumferential uniformity ratio estimate (CURE) and the systolic dyssynchrony index (SDI) parameter for the 70 subjects. The correlation after elimination of the four patients to the far left was similar as the original with $y = -4.6x + 4.8$, $r = 0.92$, $P < 0.0001$). In controls CURE ranged from 0.97 to 1.0, for SDI the range was $0.15-0.38$.

one considers the viability information as represented in the bull's eye plot in *Figure 5L*. Consequently, segments with $\geq 50\%$ transmurality of scar were excluded for the SDI calculation yielding SDI$_{viable}$. In the MI patient in *Figure 5*, the resulting SDI$_{viable}$ was 0.33, which is close to that of 0.27 in the control, i.e. within the range of normal (95% confidence interval of $0.12-0.40$). For comparison, the SDI$_{viable}$ of the LBBB patient was 1.26 indicating a potential gain of resynchronization. *Figure 2* demonstrates that the LBBB patients with reduced EF showed the highest degree of dyssynchrony as measured with CURE, SDI, or T_{max} SD. However, the SDI, in contrary to CURE and T_{max} SD, keeps the local information and thus, scared segments can be subtracted from this dyssynchrony measurement. Consequently, in Pats$_{MI}$ SDI of 0.70 ± 0.26 was significantly reduced to SDI$_{viable}$ of 0.46 ± 0.18 ($P < 0.0001$; paired *t*-test).

Reproducibility of results and method performance

As demonstrated in *Figure 7*, the inter-study, inter- and intra-observer reproducibility values were high for CURE, SDI, and T_{max} SD. The average tracking error percentages of the HARP analyses were similar in all patient groups (*Table 2*).

Discussion

The main findings of the study are as follows: (i) assessment of intraventricular dyssynchrony validated in earlier animal studies
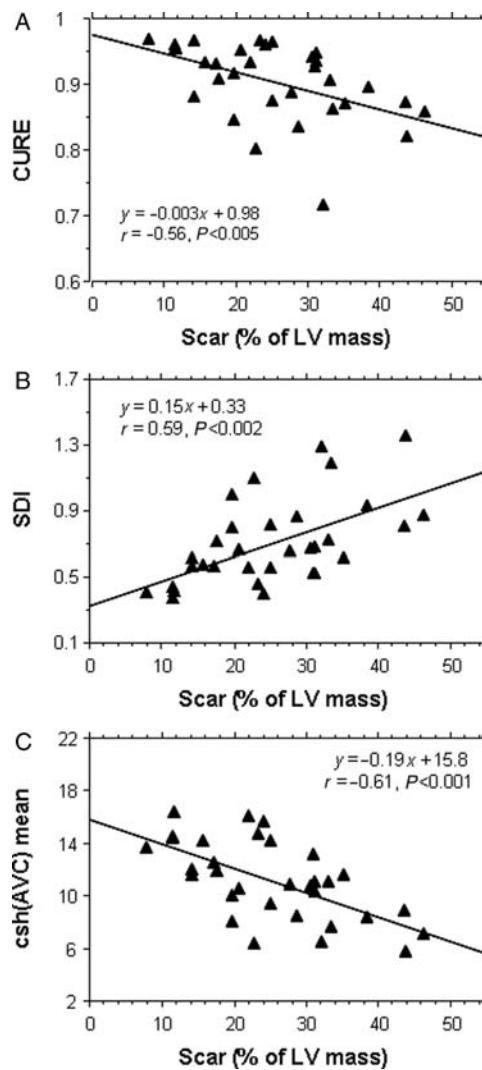

Figure 4 Linear regressions between scar mass as measured by the late gadolinium enhancement technique and different dyssynchrony and deformation parameters obtained from 3D tagging data sets of MI patients. (*A*) Circumferential uniformity ratio estimate. (*B*) systolic dyssynchrony index. (*C*) Mean csh(AVC) of the entire LV. The plots demonstrate a positive relation between the amount of scar and intraventricular dyssynchrony.

with LBBB could be transferred successfully into humans including patients with LBBB and prior MI. (ii) Despite these different underlying diseases, i.e. LBBB and ischaemic heart disease with primarily antero-septal infarctions, the observed patterns of dyssynchrony were similar between LBBB and antero-septal MI. (iii) By utilization of a segmental-based dyssynchrony parameter, viability information could be easily integrated to yield a comprehensive map for dyssynchrony and viability assessment in ischaemic heart disease, and (iv) a sufficiently high reproducibility for these dyssynchrony parameters in patients was demonstrated.
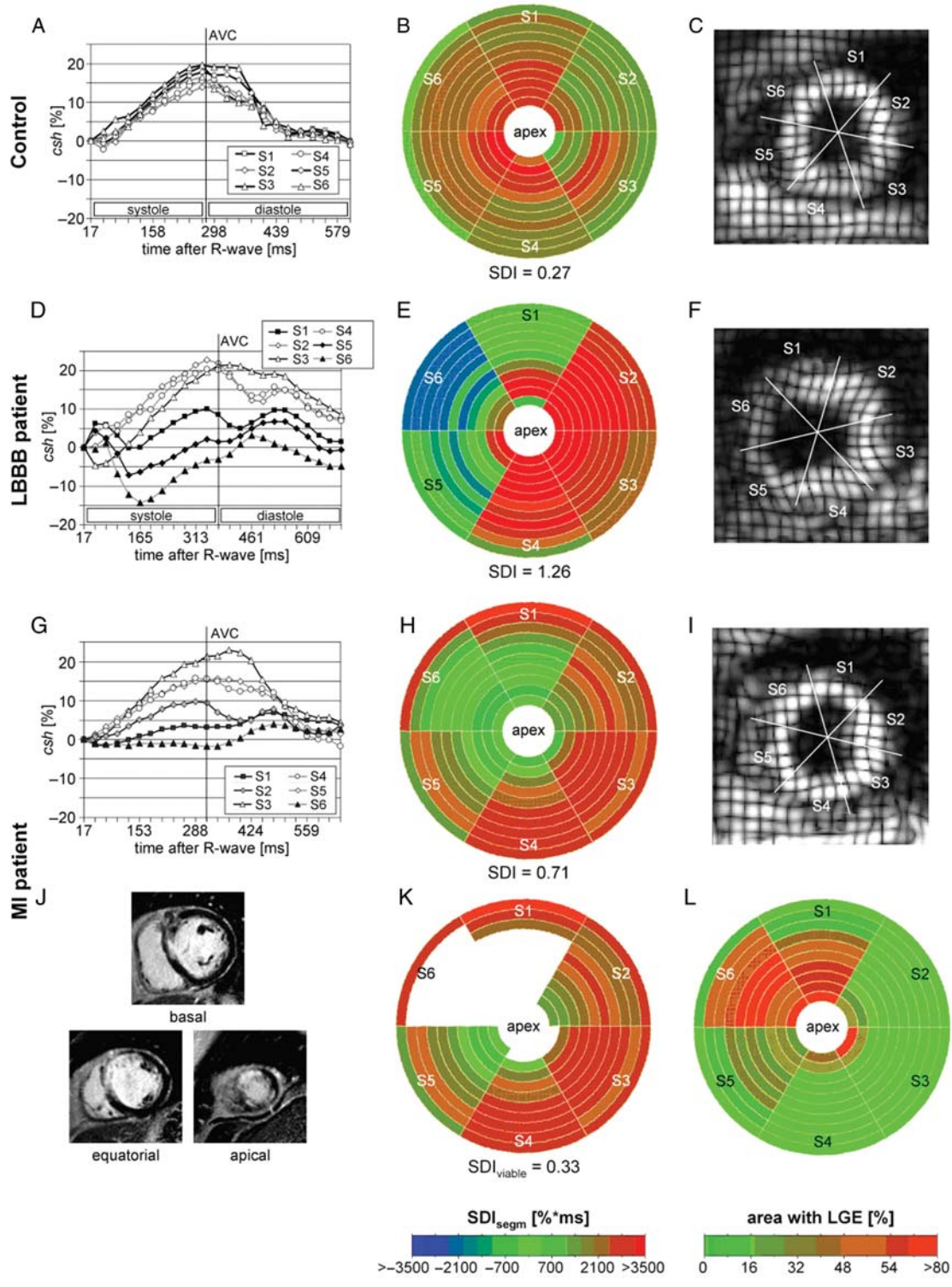
Figure 5 Representative 3D tagging results from a control (*A–C*), a left bundle branch block patient (*D–F*), and a myocardial infarction patient (*G–L*). (A, D, G) Csh over the cardiac cycle for six segments on an equatorial level. (B, E, H) Bull's eye plots of SDI$_{segm}$. (C, F, I) Short-axis slice through the 3D tagging volumes at AVC with sector definitions. (J) Three representative slices of late gadolinium enhancement (LGE) images out of 10 acquired slices are shown. (K) Bull's eye plot for SDI$_{viable}$ is shown, where segments with scar mass $\geq$ 50% are excluded. (L) Bull's eye plot of viability as derived from LGE data. Shades of red represent degree of scar transmurality. For explanation of results, see results section in the text.
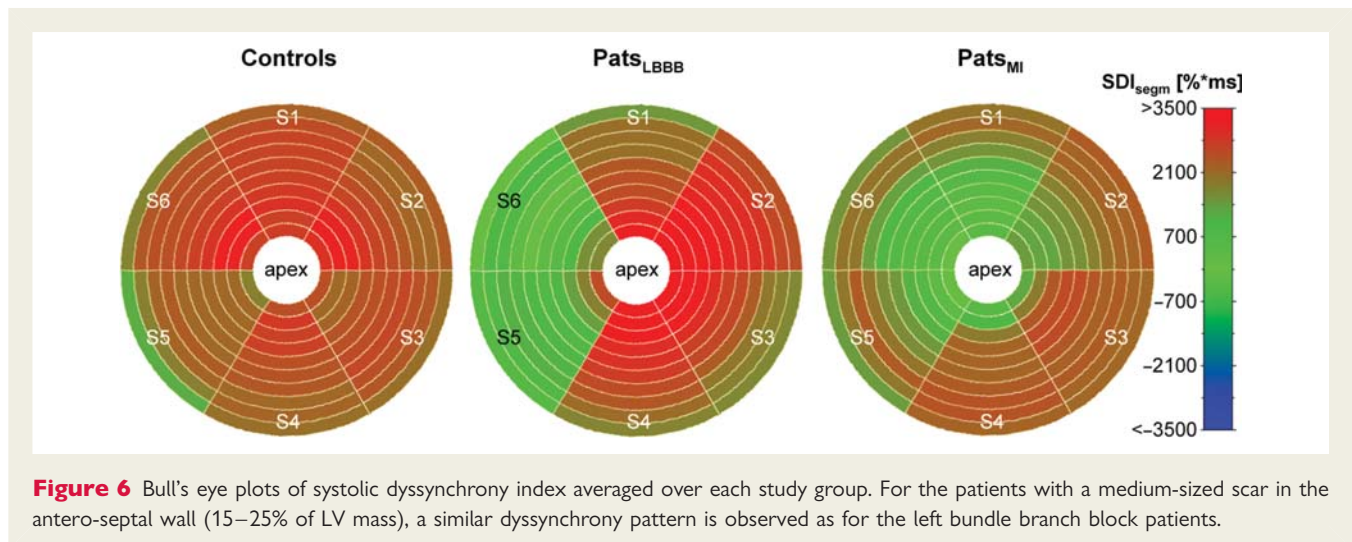
Figure 6 Bull's eye plots of systolic dyssynchrony index averaged over each study group. For the patients with a medium-sized scar in the antero-septal wall (15−25% of LV mass), a similar dyssynchrony pattern is observed as for the left bundle branch block patients.

Transfer of a dyssynchrony cardiac magnetic resonance technique into patients with various underlying cardiac pathologies

Current state-of-the-art imaging technology opens a wide spectrum of potential parameters to describe intraventricular dyssynchrony. The CURE was evaluated in several animal studies with LBBB to estimate LV dyssynchrony in longitudinal and circumferential directions.[12] Circumferential uniformity ratio estimate proved superior to other tagging parameters to identify the synchronizing effect of various pacing modes.[12,25] As a 3D data set would ideally provide the basis for such analyses, a novel 3D tagging strategy opened new perspectives by transferring the technique into humans. Other tagging techniques required ~45 min to cover the entire LV,[26] whereas the present technique acquires the complete data set in three breath-holds of 18 heartbeats duration each. The technique produced adequate data quality for analysis in 98.6% of all cases. Furthermore, the HARP approach,[27] modified to increase signal-to-noise ratio[15] and thus to increase robustness of the analysis, produced results in a few minutes, which is an important aspect of imaging techniques, if applications in clinical practice are anticipated.

Accurate and reproducible tests are of paramount importance to better understand the mechanisms of action, e.g. of CRT, in various forms of dyssynchrony. Reproducibility is also important to reliably select possible candidates for CRT. In this context, it is noteworthy that in the PROSPECT trial,[9] a large multicenter echo-based CRT trial, relevant conclusions were difficult to draw, since the imaging parameters used to quantify dyssynchrony were compromised by low reproducibility. In this respect, the presented 3D tagging CMR approach fulfils several requirements for successful clinical trials such as a short-acquisition time, adequate robustness to be performed in patients, fast semi-automatic analysis, and adequate reproducibility.

Patterns of dyssynchrony in left bundle branch block and ischaemic heart disease

Several dyssynchrony parameters such as the CURE parameter were validated primarily in animals, and often the presence of an LBBB was used as the model mimicking dyssynchrony.[18,20] Although most dyssynchrony parameters are aimed at 'condensing' the dyssynchrony information into a single quantitative measure, this approach is inherently limited by eliminating some information on the local distribution of dyssynchrony. Therefore, in addition to the CURE index, a dyssynchrony parameter was applied, which measures systolic performance in each LV segment to preserve spatial information, and then allows 'condensing' it into a single value by calculating the statistical variability of the performance in the various segments. The resulting SDI showed a similar pattern for dyssynchrony as the CURE index (*Figure 2*), with highest dyssynchrony in LBBB patients with reduced EF and a dependency of dyssynchrony on the amount of scar tissue in MI patients (*Figure 4*). The high variability of both SDI and CURE in Pats$_{LBBB}$ could indeed reflect differences in dyssynchrony among patients with LBBB. Animal studies in LBBB demonstrated substantial differences in adaptive remodelling of hearts subjected to LBBB,[3] which could also cause differences in dyssynchrony, even when evoked by the same conduction disturbance, i.e. LBBB.

Relationship between QRS duration and cardiac magnetic resonance dyssynchrony parameters

QRS duration of $\geq$ 120 ms is a major criterion among others to select patients for CRT combining into a class I indication.[6] In this study, QRS duration showed a weak inverse relationship with EF indicating that LV dyssynchrony, which goes along with intraventricular unloading phenomena[1,2] may be a reason among others to reduce EF and thus, LV pumping efficiency. In the patients with reduced EF after MI or with LBBB, the proposed SDI$_{viable}$ parameter correlated weakly with QRS duration, whereas SDI and CURE did not. This finding may provide indirect evidence, why
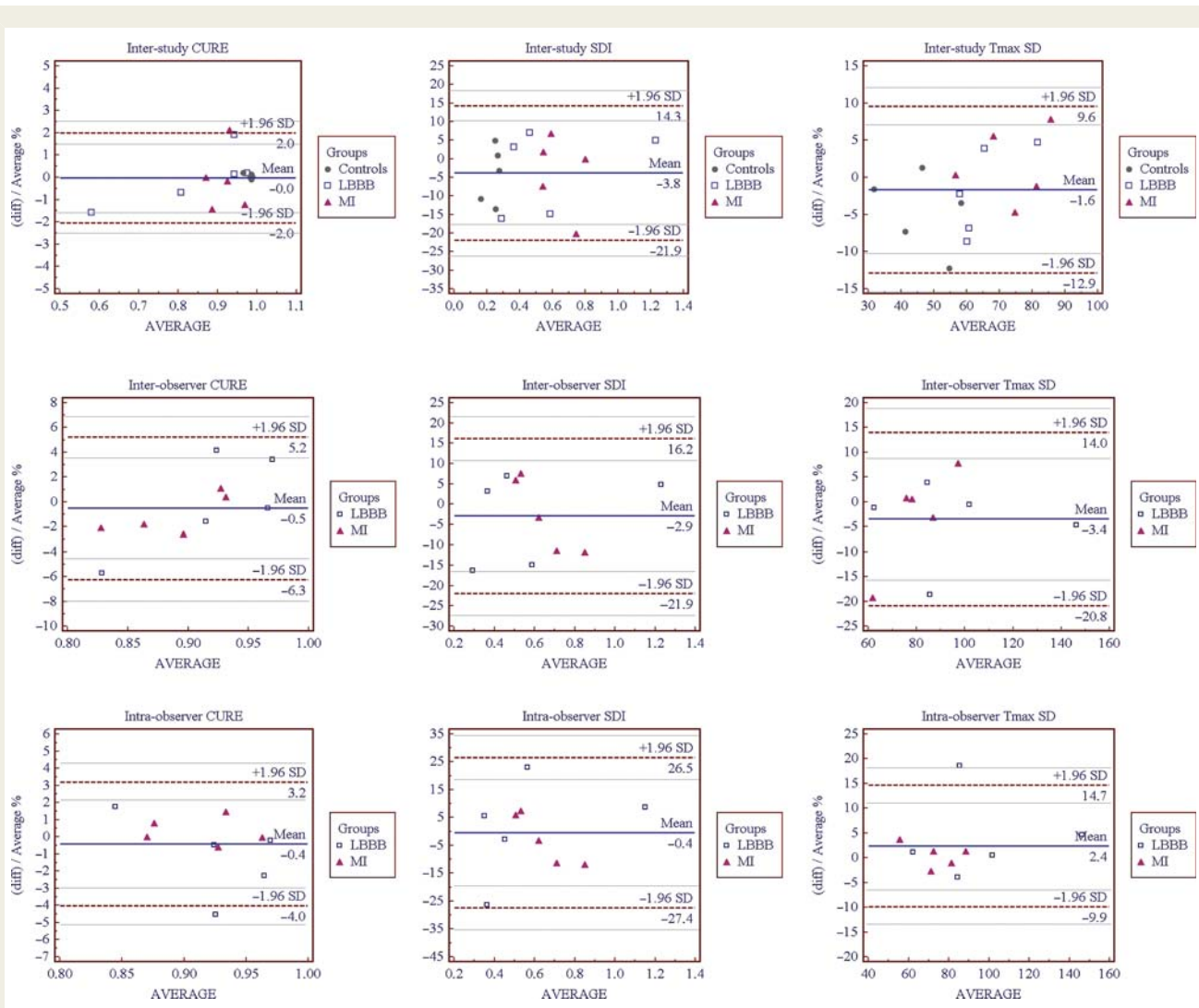
Figure 7 Inter-study (upper row), inter-observer (centre row), and intra-observer reproducibility (lower row) of parameters measuring left ventricular dyssynchrony represented as Bland−Altman plots. Dashed horizontal lines indicate ± 95% limits of agreement, bold lines represent mean differences (equal to bias). Since the sample sizes for these reproducibility measurements were rather small, the 95% confidence intervals (grey lines) for the limits of agreement (dashed lines) are also given. The upper and lower limits of agreement for inter-study-circumferential uniformity ratio estimate (CURE) are: 1.5−2.5% and −1.6% to −2.5%, respectively, for inter-study-systolic dyssynchrony index (SDI): 10.1−18.5% and −26.1 to −17.7%, respectively, for inter-study-T_{max} SD: 7.0−12.2% and −15.5% to −10.3%, respectively. For inter-observer-CURE: 3.5−6.9% and −8.0% to −4.6%, respectively; for inter-observer-SDI: 10.5−21.8% and −27.6% to −16.3%, respectively; for inter-observer-T_{max} SD: 8.9−19.2% and −26.0% to −15.7%, respectively. For intra-observer-CURE: 2.1−4.3% and −5.1% to −3.0%, respectively; for intra-observer-SDI: 18.5−34.4% and −35.5% to −19.4%, respectively; for intra-observer-T_{max} SD: 11.0−18.3% and −13.6% to −6.3%, respectively.

QRS duration is adding valuable information to select patients for CRT.

Integration of viability information into a comprehensive approach to assess dyssynchrony

The similarity of dyssynchrony patterns in LBBB and antero-septal infarcts emphasize the importance of integrating viability information into maps of dyssynchrony. The proposed SDI as any segmental-based approach to quantify dyssynchrony is ideal to integrate viability information. Assuming that a ≥ 50% scar trans-murality in a given segment would prevent systolic contractions, such segments can easily be eliminated from the calculation of a global dyssynchrony estimate. For example, in the patient after MI given in *Figure 5*, the SDI$_{viable}$ was 0.33, which is comparable to the SDI$_{viable}$ of 0.27 obtained in the healthy control (95% confidence interval of controls: 0.12−0.40). Consequently, the dyssynchrony parameter SDI$_{viable}$ in this patient after MI would indicate little or no potential improvement in contractile segmental function with pacing. Although a low SDI$_{viable}$ would indicate little chance to benefit from CRT, future outcome studies will be

needed to show whether a high SDI$_{viable}$ can predict responsiveness to CRT. It should be mentioned that any threshold of scar transmurality can be applied to calculate and plot SDI$_{viable}$. In particular, not only scar transmurality, but also absolute thickness of scar and viable rim tissue are likely to determine responsiveness to pacing. To further increase the likelihood to predict responsiveness to CRT, the proposed bull's eye plot of SDI$_{viable}$ could also be overlayed with an MR angiogram of the venous system for optimal planning of the pacing site.

Limitations

The CURE index is well validated in LBBB in animal models. Therefore, it was used in the present study as the reference for comparisons with other parameters of dyssynchrony such as the SDI. This means that no other 'gold standard' for quantification of dyssynchrony was applied in this study for the LBBB patients. Similarly, for the Pats$_{MI}$, no other measures of reference for dyssynchrony were performed which is mainly explained by the lack of any absolutely established measure to quantify dyssynchrony in these patients.

The 3D nature of the tagging data in the patients would allow for a multi-directional analysis of strain in the LV, i.e. not only in circumferential, but also in longitudinal and radial directions. However, previous data indicate that longitudinal strain is less sensitive to dyssynchrony than circumferential strain.[12]

In the Pats$_{MI}$ group, there is a relatively large portion of antero-septal infarcts, which limits the applicability of the study findings to the overall post-MI population. This disproportion towards larger antero-septal infarcts may be due to a higher rate of symptomatic patients with these infarcts, which consequently may lead to a higher rate of referrals for invasive diagnostics and treatment. Assuming that scar tissue would not benefit from pacing, the antero-septal infarcts are then an important model to demonstrate, that these patients show a similar dyssynchrony pattern as in LBBB, which is, however, readily discernable by a comprehensive assessment of viability, i.e. by measuring SDI$_{viable}$.

Conclusions

Dyssynchrony patterns due to LBBB or scar formation in the LV were quantified by 3D-tagging CMR yielding global and segmental dyssynchrony parameters. The proposed segmental dyssynchrony approach also allowed integrating viability information resulting in SDI$_{viable}$, which quantifies dyssynchrony in viable tissue only. Despite similar dyssynchrony patterns in LBBB and patients with antero-septal MI, SDI$_{viable}$ unambiguously discriminated these patient populations. Future studies are warranted to test the value of such an integrated dyssynchrony—viability approach to predict responsiveness to resynchronization.

Acknowledgements

Appendix

Calculation of the cure index

Csh was plotted vs. spatial position for each slice and in each time frame. The plots were subjected to Fourier analysis, and CURE was calculated as follows: CURE $= (A_0^2/[A_0^2 + 2A_1^2])^{1/2}$, where A_0^2 and A_1^2 are the sums over space and time of the zero and first-order power terms, respectively. Thus, CURE represents a measure for the amount of oscillation in the plots of csh vs. spatial position. Circumferential uniformity ratio estimate ranged from 0 (pure dyssynchrony) to 1 (synchronous).

Calculation of the systolic dyssynchrony index

The regional estimate in each segment (SDI$_{segm}$) was defined as the area under curve of csh(t) from $t = 1/3$AVC to $t =$ AVC:

$$\text{SDI}_{segm} = \int_{1/3\text{AVC}}^{\text{AVC}} \text{csh}(t)\, dt$$

Measuring the area under curve is less susceptible to noise than analysing a single time point during contraction only.

The SD of the obtained values of all segments over the LV divided by the LV mean value defined SDI for global measurement of LV dyssynchrony:

$$\text{SDI} = \frac{\text{SD}(\text{SDI}_{segm})}{\text{mean}(\text{SDI}_{segm})}$$

Harmonic phase tracking performance

The HARP tracking performance was determined by counting the number of tracking errors during the HARP post-processing of each data set. A tracking error of a material point from one time frame to the next could be caused by the following reasons:[14] (i) non-convergence of the HARP algorithm; (ii) the displacement exceeded the tagging distance; (iii) the displacement of neighbouring points was significantly different. Tracking errors were detected automatically and corrected by the software based on the motion of correctly identified neighbouring points.

References

1. Smalling RW, Ekas RD, Felli PR, Binion L, Desmond J. Reciprocal functional interaction of adjacent myocardial segments during regional ischemia: an intraventricular loading phenomenon affecting apparent regional contractile function in the intact heart. *J Am Coll Cardiol* 1986;**7**:1335–1346.

2. Ryf S, Rutz AK, Boesiger P, Schwitter J. Is post-systolic shortening a reliable indicator of myocardial viability? An MR tagging and late-enhancement study. *J Cardiovasc Magn Reson* 2006;**8**:445–451.

3. Vernooy K, Verbeek XA, Peschar M, Crijns HJ, Arts T, Cornelussen RN, Prinzen FW. Left bundle branch block induces ventricular remodelling and functional septal hypoperfusion. *Eur Heart J* 2005;**26**:91–98.

4. Rosenbush S, Ruggie N, Turner D, von Behren P, Denes P, Fordham E, Groch M, Messer J. Sequence and timing of ventricular wall motion in patients with bundle branch block. *Circulation* 1982;**66**:1113–1119.

5. Kass DA. Cardiac resynchronization therapy. *J Cardiovasc Electrophysiol* 2005;**16**(Suppl. 1):S35–S41.

6. Vardas P, Auricchio A, Blanc J, Daubert J, Drexler H, Ector H, Gasparini M, Linde C, Bello F, Oto A, Sutton R, Trusz-Gluza M. Guidelines for cardiac pating and cardiac resynchronization therapy of the European Society of Cardiology. *Europace* 2007;**9**:959–998.

7. Bax JJ, Bleeker GB, Marwick TH, Molhoek SG, Boersma E, Steendijk P, van der Wall EE, Schalij MJ. Left ventricular dyssynchrony predicts response and prognosis after cardiac resynchronization therapy. *J Am Coll Cardiol* 2004;**44**:1834–1840.

8. Sogaard P, Egeblad H, Kim WY, Jensen HK, Pedersen AK, Kristensen BO, Mortensen PT. Tissue Doppler imaging predicts improved systolic performance and reversed left ventricular remodeling during long-term cardiac resynchronization therapy. *J Am Coll Cardiol* 2002;**40**:723–730.

9. Chung ES, Leon AR, Tavazzi L, Sun JP, Nihoyannopoulos P, Merlino J, Abraham WT, Ghio S, Leclercq C, Bax JJ, Yu CM, Gorcsan J III, St John Sutton M, De Sutter J, Murillo J. Results of the Predictors of Response to CRT (PROSPECT) trial. *Circulation* 2008;**117**:2608–2616.

10. Tecelao SR, Zwanenburg JJ, Kuijer JP, de Cock CC, Germans T, van Rossum AC, Marcus JT. Quantitative comparison of 2D and 3D circumferential strain using MRI tagging in normal and LBBB hearts. *Magn Reson Med* 2007;**57**:485–493.

11. Nelson GS, Curry CW, Wyman BT, Kramer A, Declerck J, Talbot M, Douglas MR, Berger RD, McVeigh ER, Kass DA. Predictors of systolic augmentation from left ventricular preexcitation in patients with dilated cardiomyopathy and intraventricular conduction delay. *Circulation* 2000;**101**:2703–2709.

12. Helm RH, Leclercq C, Faris OP, Ozturk C, McVeigh E, Lardo AC, Kass DA. Cardiac dyssynchrony analysis using circumferential versus longitudinal strain: implications for assessing cardiac resynchronization. *Circulation* 2005;**111**:2760–2767.

13. Rutz AK, Ryf S, Plein S, Boesiger P, Kozerke S. Accelerated whole-heart 3D CSPAMM for myocardial motion quantification. *Magn Reson Med* 2008;**59**:755–763.

14. Osman NF, Kerwin WS, McVeigh ER, Prince JL. Cardiac motion tracking using CINE harmonic phase (HARP) magnetic resonance imaging. *Magn Reson Med* 1999;**42**:1048–1060.

15. Ryf S, Tsao J, Schwitter J, Stuessi A, Boesiger P. Peak-combination HARP: a method to correct for phase errors in HARP. *J Magn Reson Imaging* 2004;**20**:874–880.

16. Kim RJ, Wu E, Rafael A, Chen EL, Parker MA, Simonetti O, Klocke FJ, Bonow RO, Judd RM. The use of contrast-enhanced magnetic resonance imaging to identify reversible myocardial dysfunction. *N Engl J Med* 2000;**343**:1445–1453.

17. Knuesel PR, Nanz D, Wyss C, Buechi M, Kaufmann PA, von Schulthess GK, Luscher TF, Schwitter J. Characterization of dysfunctional myocardium by positron emission tomography and magnetic resonance: relation to functional outcome after revascularization. *Circulation* 2003;**108**:1095–1100.

18. Leclercq C, Faris O, Tunin R, Johnson J, Kato R, Evans F, Spinelli J, Halperin H, McVeigh E, Kass DA. Systolic improvement and mechanical resynchronization does not require electrical synchrony in the dilated failing heart with left bundle-branch block. *Circulation* 2002;**106**:1760–1763.

19. Russel IK, Zwanenburg JJ, Germans T, Marcus JT, Allaart CP, de Cock CC, Gotte MJ, van Rossum AC. Mechanical dyssynchrony or myocardial shortening as MRI predictor of response to biventricular pacing? *J Magn Reson Imaging* 2007;**26**:1452–1460.

20. Byrne MJ, Helm RH, Daya S, Osman NF, Halperin HR, Berger RD, Kass DA, Lardo AC. Diminished left ventricular dyssynchrony and impact of resynchronization in failing hearts with right versus left bundle branch block. *J Am Coll Cardiol* 2007;**50**:1484–1490.

21. Ypenburg C, Schalij MJ, Bleeker GB, Steendijk P, Boersma E, Dibbets-Schneider P, Stokkel MP, van der Wall EE, Bax JJ. Extent of viability to predict response to cardiac resynchronization therapy in ischemic heart failure patients. *J Nucl Med* 2006;**47**:1565–1570.

22. Liu YL, Riederer SJ, Rossman PJ, Grimm RC, Debbins JP, Ehman RL. A monitoring, feedback, and triggering system for reproducible breath-hold MR imaging. *Magn Reson Med* 1993;**30**:507–511.

23. Zwanenburg JJ, Gotte MJ, Marcus JT, Kuijer JP, Knaapen P, Heethaar RM, van Rossum AC. Propagation of onset and peak time of myocardial shortening in time of myocardial shortening in ischemic versus nonischemic cardiomyopathy: assessment by magnetic resonance imaging myocardial tagging. *J Am Coll Cardiol* 2005;**46**:2215–2222.

24. Bland JM, Altman DG. Statistical methods for assessing agreement between two methods of clinical measurement. *Lancet* 1986;**1**:307–310.

25. Helm RH, Byrne M, Helm PA, Daya SK, Osman NF, Tunin R, Halperin HR, Berger RD, Kass DA, Lardo AC. Three-dimensional mapping of optimal left ventricular pacing site for cardiac resynchronization. *Circulation* 2007;**115**:953–961.

26. Wyman BT, Hunter WC, Prinzen FW, Faris OP, McVeigh ER. Effects of single- and biventricular pacing on temporal and spatial dynamics of ventricular contraction. *Am J Physiol Heart Circ Physiol* 2002;**282**:H372–H379.

27. Garot J, Bluemke DA, Osman NF, Rochitte CE, McVeigh ER, Zerhouni EA, Prince JL, Lima JA. Fast determination of regional myocardial strain fields from tagged cardiac images using harmonic phase MRI. *Circulation* 2000;**101**:981–988.